Radio Science, Volume 22, Number 2, Pages 292–306, March–April 1987

A semi-empirical low-latitude ionospheric model

David N. Anderson

Air Force Geophysics Laboratory, Hanscom Air Force Base, Massachusetts

Michael Mendillo and Bruce Herniter

Astronomy Department, Boston University, Massachusetts

(Received July 29, 1986; revised November 11, 1986; accepted November 11, 1986.)

Since current empirical models specifying low-latitude electron density profiles severely underestimate the daytime plasma density scale-height and total electron content (TEC) values, a semi-empirical low-latitude ionospheric model (SLIM) has been developed which is not only computationally fast, but also more realistic. Electron density profiles (180–1800 km) are theoretically calculated as a function of latitude (every 2° between 24 N and 24 S dip latitude) and local time (every half hour, over 24 hours LT) by solving the time-dependent plasma continuity equation. Using simple exponential functions, sets of coefficients are then generated which reproduce these individual profiles. The coefficients themselves are easily stored, quickly retrieved and form the basis for a fast, portable, semi-empirical computer code. This paper describes briefly the input parameters used to theoretically calculate the profiles and the procedures used to generate the coefficients. The SLIM profiles are compared with the Chiu and Bent empirical models for equinox, solar maximum conditions, while calculated 6300 Å airglow intensities and TEC values are compared with available observations. The SLIM profiles, their coefficients, TEC and 6300 Å airglow intensities are available in tabular and computer formats.

1. INTRODUCTION

1.1. *Background*

Current empirical models of the low-latitude ionospheric *F* region [*Llewellyn and Bent*, 1973; *Chiu*, 1975; *Rawer*, 1981] can severely underestimate the daytime plasma density scale height and total electron content (TEC) when compared with actual observations. As illustrated in Figure 1, the International Reference Ionosphere (IRI) described by *Rawer* [1981] yields daytime TEC values which are 50% lower than observed TEC values at Manila (dip 14.5° N) in January 1982 [*McNamara*, 1984]. Some improvement occurs when the Bent topside model is incorporated with the IRI bottomside models but the predicted values are still lower than observed. Substantial improvement is achieved when theoretically calculated profiles [*Anderson*, 1973] are used to predict TEC values. The reason is that vertical plasma transport by upward **E** × **B** drift produces both topside and bottomside profiles which are much broader (thicker) than Chapman-like profiles.

To theoretically calculate electron density profiles whenever they are needed, however, is prohibitively time-consuming on even the fastest computer. An alternate solution to this problem is to theoretically calculate electron density profiles as a function of latitude and local time and then generate coefficients which produce these profiles. The coefficients themselves are easily stored, quickly retrieved and form the basis for a fast, portable computer code which will produce realistic low-latitude *F* region electron density profiles. The results of this technique are called the semi-empirical low-latitude ionospheric model (SLIM).

Using the techniques described by *Anderson* [1973] electron densities as a function of altitude, latitude and local time are calculated by solving the time-dependent ion (O^+) continuity equation numerically. The effects of production by photoionization, loss through charge exchange with N_2 and O_2 and transport by diffusion, neutral winds and vertical **E** × **B** drift are included. Because **E** × **B** drifts play such an important role in determining the electron density distribution [*Hanson and Moffett*, 1966; *An-*

Paper number 6S0657.
0048-6604/87/006S-0657$08.00

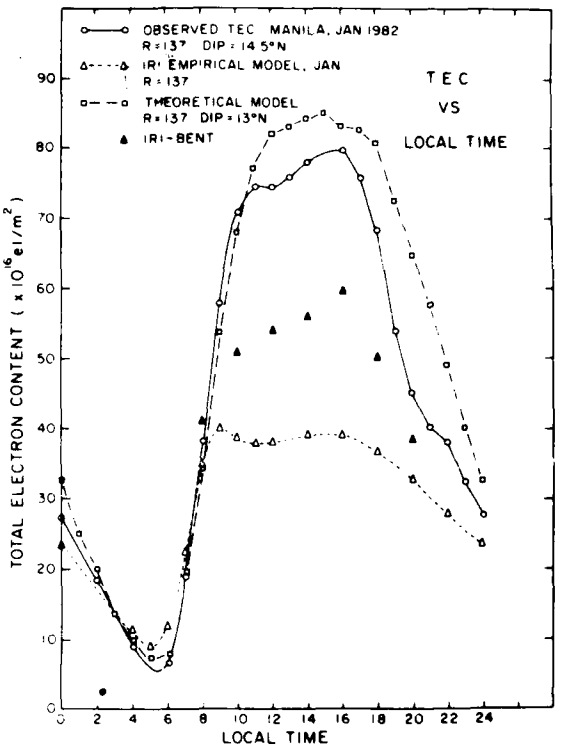

Fig. 1. A comparison between observed, predicted, and theoretically calculated total electron content (TEC) values at Manila as a function of local time for January 1982. R is the sunspot number and DIP refers to the angle the geomagnetic field line makes with the local horizon.

derson, 1973] and have a seasonal and solar cycle dependence [*Fejer et al.*, 1979], the calculations are carried out for equinox and solstice conditions for both solar cycle maximum and minimum periods.

Once electron density profiles are obtained, they are normalized to the peak electron density, N_{max}, and appropriate coefficients which reproduce the normalized profiles (180–1800 km) every half hour local time and every 2° dip latitude are calculated. To regenerate density profiles simply requires specifying N_{max} internally (that is, reuse of the theoretical N_{max} values) or by externally using an empirical model such as *CCIR* [1978] or observed f_0F_2 values, and then choosing the calculated coefficients applicable to the specified latitude and local time location. In the following sections, we describe briefly the various input parameters which were used in calculating theoretically the electron density profiles from the time-dependent continuity equation. In the last sections we compare (1) the current Chiu and Bent empirical profiles with SLIM profiles at specific latitudes and local times for equinox, solar cycle maximum conditions, (2) calculated and observed 6300-Å airglow intensities, and (3) calculated and observed TEC values.

1.2. *Model calculations*

The ion (O^+) continuity equation is given by

$$\frac{\partial N_i}{\partial t} + \nabla \cdot (N_i \mathbf{V}_i) = P_i - L_i \tag{1}$$

where $N_i (= N_e)$ is the ion density; P_i, the ion production rate; L_i the ion loss rate; and $\mathbf{V}_i$, the ion transport velocity. In the ionosphere, plasma is transported along geomagnetic field lines by diffusion and neutral winds and perpendicular to field lines primarily by $\mathbf{E} \times \mathbf{B}$ drift [*Kendall and Pickering*, 1967]. Solving (1) at low latitudes is facilitated by transforming the independent coordinates r, θ and ϕ to a coordinate system parallel and perpendicular to $\mathbf{B}$ [see *Anderson*, 1973]. Equation (1) can be written

$$\frac{\partial N_i}{\partial t} + \mathbf{V}_{i_\perp} \cdot \nabla N_i = P_i - L_i - \nabla \cdot (N_i \mathbf{V}_i) - N_i \nabla \cdot \mathbf{V}_{i_\perp} \tag{2}$$

where $\mathbf{V}_{i_\perp}$ is given by $\mathbf{E} \times \mathbf{B}\, B^2$ and $\mathbf{V}_i$ includes the effects of plasma diffusion and neutral wind. The right-hand side of the equation involves terms which are second order in the coordinate parallel to $\mathbf{B}$. The left-hand side of (2) is the time rate of change of plasma density in a frame of reference which drifts

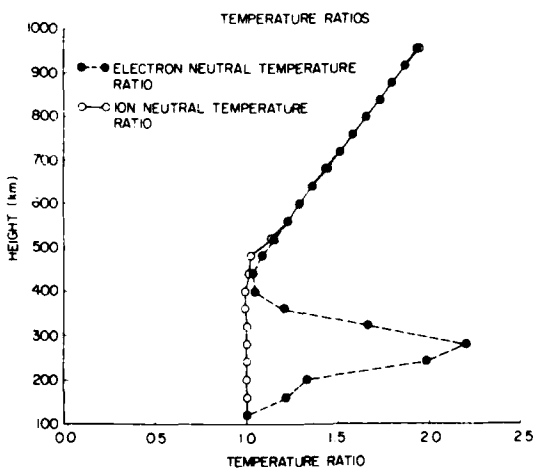

Fig. 2. Ion-neutral and electron-neutral temperature ratios as a function of altitude. The neutral temperature is adopted from the MSIS model atmosphere (see text for details).

UNCLASSIFIED
SECURITY CLASSIFICATION OF THIS PAGE

ADA201772

REPORT DOCUMENTATION PAGE

Form Approved OMB No. 0704-0188

1a. REPORT SECURITY CLASSIFICATION: Unclassified	1b. RESTRICTIVE MARKINGS
2a. SECURITY CLASSIFICATION AUTHORITY	3. DISTRIBUTION/AVAILABILITY OF REPORT: Approved for public release; distribution unlimited
2b. DECLASSIFICATION/DOWNGRADING SCHEDULE	
4. PERFORMING ORGANIZATION REPORT NUMBER(S): AFGL-TR-88-0282	5. MONITORING ORGANIZATION REPORT NUMBER(S)
6a. NAME OF PERFORMING ORGANIZATION: Air Force Geophysics Laboratory; 6b. OFFICE SYMBOL (If applicable): LIS	7a. NAME OF MONITORING ORGANIZATION
6c. ADDRESS (City, State, and ZIP Code): Hanscom AFB, Massachusetts 01731-5000	7b. ADDRESS (City, State, and ZIP Code)
8a. NAME OF FUNDING/SPONSORING ORGANIZATION; 8b. OFFICE SYMBOL (If applicable)	9. PROCUREMENT INSTRUMENT IDENTIFICATION NUMBER
8c. ADDRESS (City, State, and ZIP Code)	10. SOURCE OF FUNDING NUMBERS: PROGRAM ELEMENT NO. 62101F; PROJECT NO. 2310; TASK NO. G9; WORK UNIT ACCESSION NO. 03

11. TITLE (Include Security Classification)

A Semi-Empirical Low-Latitude Ionospheric Model

12. PERSONAL AUTHOR(S)

David N. Anderson, Michael Mendillo* and Bruce Hermiter*

13a. TYPE OF REPORT	13b. TIME COVERED	14. DATE OF REPORT (Year, Month, Day)	15. PAGE COUNT
Reprint	FROM _____ TO _____	1988 October 6	15

16. SUPPLEMENTARY NOTATION

Reprinted from Radio Science, Volume 22, Number 2, Pages 292-306, March-April 1987

*Astronomy Department, Boston University, Boston, MA 02215

17. COSATI CODES		
FIELD	GROUP	SUB-GROUP

18. SUBJECT TERMS (Continue on reverse if necessary and identify by block number)

Low-Latitude Ionosphere
Theoretical Model
E x B Drifts

19. ABSTRACT (Continue on reverse if necessary and identify by block number)

Since current empirical models specifying low-latitude electron density profiles severely underestimate the daytime plasma density scale height and total electron content (TEC) values, a semi-empirical low-latitude ionospheric model (SLIM) has been developed which is not only computationally fast, but also more realistic. Electron density profiles (180-1800 km) are theoretically calculated as a function of latitude (every 2° between 24°N and 24°S dip latitude) and local time (every half hour, over 24 hours LT) by solving the time-dependent plasma continuity equation. Using simple exponential functions, sets of coefficients themselves are easily stored, quickly retrieved and form the basis for a fast, portable, semi-empirical computer code. This paper describes briefly the input parameters used to theoretically calculate the profiles and the procedures used to generate the coefficients. The SLIM profiles are compared with the Chiu and Bent empirical models for equinox, solar maximum conditions, while calculated at 6300 Å airglow intensities and TEC values are compared with available observations. The SLIM profiles, their coefficients, TEC and 6300 Å airglow

20. DISTRIBUTION/AVAILABILITY OF ABSTRACT	21. ABSTRACT SECURITY CLASSIFICATION
☒ UNCLASSIFIED/UNLIMITED ☐ SAME AS RPT. ☐ DTIC USERS	UNCLASSIFIED
22a. NAME OF RESPONSIBLE INDIVIDUAL: David N. Anderson	22b. TELEPHONE (Include Area Code): (617) 377-3982 — 22c. OFFICE SYMBOL: LIS

DD Form 1473, JUN 86 — Previous editions are obsolete. — SECURITY CLASSIFICATION OF THIS PAGE

UNCLASSIFIED

intensities are available in tabular and computer formats. (Reprints, j'hal)

with the **E** × **B** drift velocity. Equation (2) is solved numerically to give ion densities as a function of altitude, latitude and local time (see *Moffett* [1979] for a review of transformations and numerical solutions).

The set of coefficients for the ion continuity equation is obtained from models of the neutral composition, ion and electron temperatures, and production, loss and diffusion rates as well as **E** × **B** drift and neutral wind models. Briefly, the models are the following:

1. The MSIS [*Hedin*, 1983] neutral atmospheric model is used to calculate N_2, O_2, and O densities and the neutral temperature, T_n, as a function of altitude, latitude and local time. An $F10.7$ cm flux of 180 units is chosen to represent solar cycle maximum period, and 70 units for solar minimum conditions. Average geomagnetic conditions were chosen by setting $Ap = 15$ in the MSIS model.

2. Production and diffusion rates are similar to those used by *Anderson* [1973]. For the photoionization rate at the top of the atmosphere, P_x, a value of 5.5×10^{-7} s^{-1} represents solar cycle maximum conditions, with a value of 2.3×10^{-7} s^{-1}, for solar minimum conditions. The loss rate coefficients are adopted from *Torr and Torr* [1979].

3. Plasma temperatures were chosen by adopting T_e/T_n and T_i/T_n ratios as a function of local time, altitude and season from the IRI model and then applying those ratios to the T_n results obtained from MSIS. Figure 2 illustrates the height variation of the ratios for the sunspot maximum equinox case.

4. The vertical **E** × **B** drift velocity observed by *Woodman* [1970] is essential in producing and maintaining the electron density distribution observed near the magnetic equator. We adopt six vertical drift models to represent, respectively, three seasons (equinox, summer and winter solstices) at solar cycle maximum and solar cycle minimum periods. The different drift patterns are based primarily on the Jicamarca incoherent scatter radar observations reported by *Fejer et al.* [1979]. We have assumed the vertical drift velocity is independent of altitude. The east-west component of **E** × **B** drift reported by *Fejer et al.* [1981] is neglected in the calculations because its effect on electron density profiles is negligible [*Anderson*, 1981]. Figures 3*a*, 3*b* and 3*c* display the diurnal variation in drift for the equinox, June solstice and December solstice cases, for solar maximum and minimum, respectively.

5. The geomagnetic field is represented by a dipole model whose axis is aligned with the earth's rotational axis. Although we incorporate **E** × **B** drift models appropriate to the American sector (where the dip equator lies 12° south of the geographic

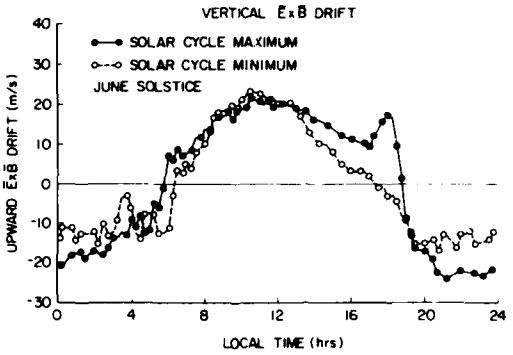

Fig. 3*b*. Vertical **E** × **B** plasma drift as a function of local time during solar cycle maximum and minimum periods for June solstice conditions.

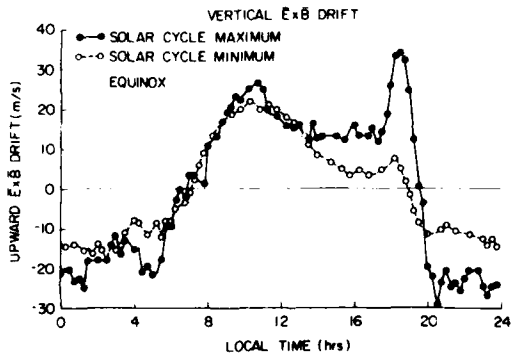

Fig. 3*a*. Vertical **E** × **B** plasma drift as a function of local time during solar cycle maximum and minimum periods for equinox conditions.

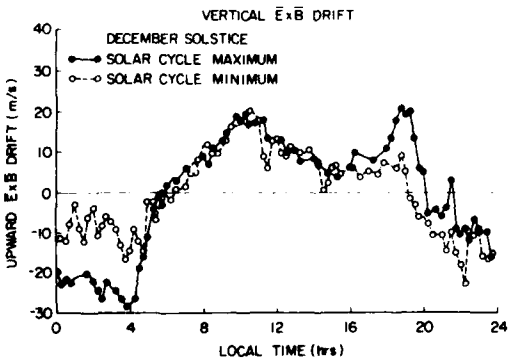

Fig. 3*c*. Vertical **E** × **B** plasma drift as a function of local time during solar cycle maximum and minimum periods for December solstice conditions.

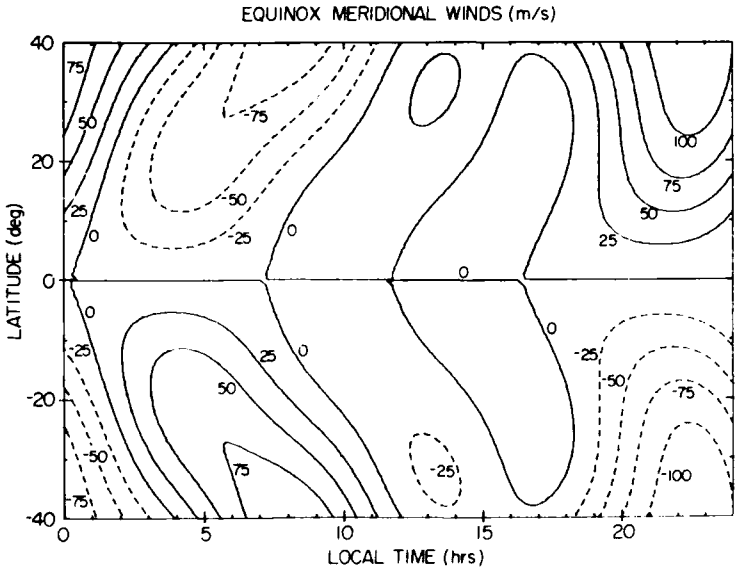

Fig. 4*a*. Contour plot of meridional neutral wind as a function of latitude and local time for equinox periods. Positive values represent north-to-south winds.

equator), longitude effects are not addressed at this time. Further development of the model will include a tilted dipole geomagnetic field with declination specified over the regions of interest.

6. A simple analytic formulation for the meridional neutral wind field is adopted which makes use of observations and theory. It is constructed on the basis of observed mean (DC), diurnal (24-hour), semidiurnal (12-hour), and terdiurnal (8-hour) harmonics at Arecibo (18°N), Millstone Hill (42°N) and St.

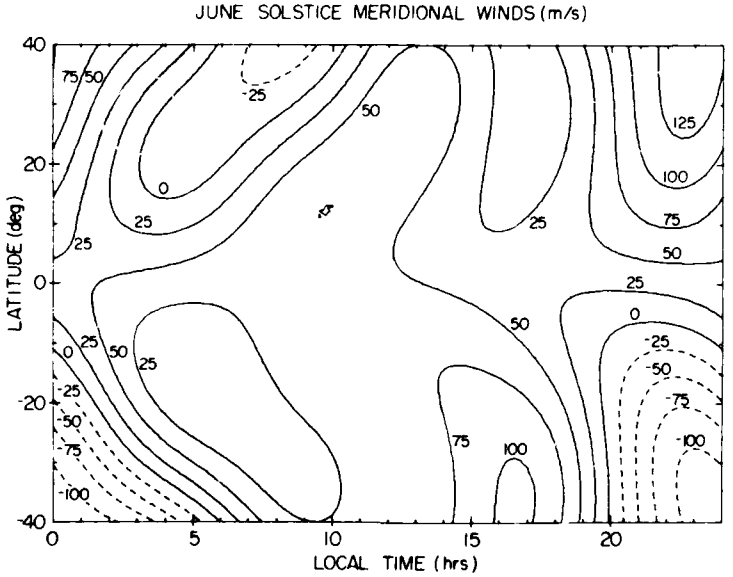

Fig. 4*b*. Contour plot of meridional neutral wind as a function of latitude and local time for June solstice periods. Positive values represent north-to-south winds.

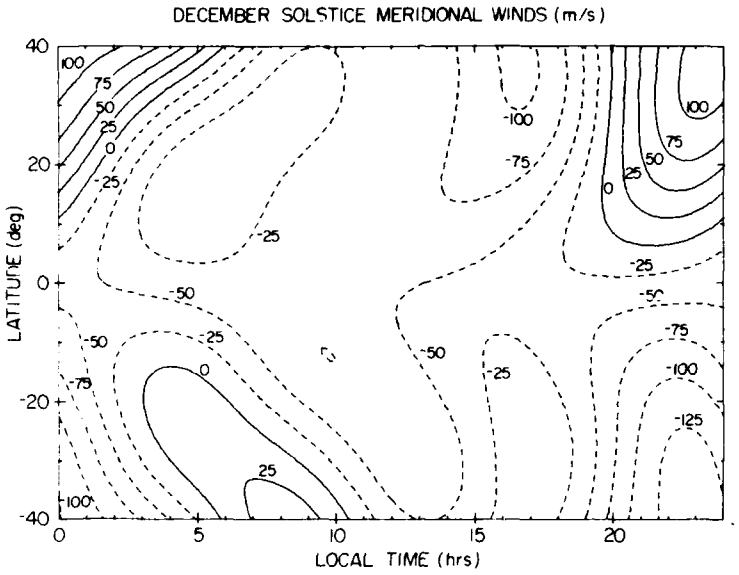

Fig. 4c. Contour plot of meridional neutral wind as a function of latitude and local time for December solstice periods. Positive values represent north-to-south winds.

Santin (45 N), with latitude variations of amplitude and phase obtained from theoretical (numerical) simulations [*Forbes*, 1982*a*, *b*]. The general latitudinal pattern assumed is guided by the tidal calculations of *Forbes* [1982*a*, *b*] and the zonal mean velocities presented by *Roble et al.* [1977]. The analytic expressions, valid only for latitudes $|\theta| \leq 45^\circ$, are given in the appendix for equinox, December solstice and June solstice periods.

For solstice conditions, the diurnal component, V_{24}, is shifted 10° in latitude in the direction of the solar bulge (consistent with Forbes). The *Roble et al.* [1977] mean meridional winds, V_0, during solstice are shifted downwards by about 40 m/s so that the transequatorial amplitudes are of the order 50 m/s and the winter hemisphere reversal occurs near Millstone Hill.

The solstitial modifications to the mean and diurnal components adequately account for the main features of the observed seasonal-latitudinal dependence of the meridional wind for our purposes. Seasonal variations in the semidiurnal and terdiurnal components are neglected. Figures 4*a*, 4*b*, and 4*c* give contour plots of the overall wind model spanning the simulation region where positive values represent north-to-south winds. Finally, it should be noted that while EUV varies markedly over a solar cycle, the associated variations in ion drag suppress solar cycle variations in the tidal winds, although neutral temperatures vary considerably. Therefore, we have assumed the current wind model parameterization to be independent of solar activity.

2. THE SEMI-EMPIRICAL APPROACH

2.1. *The SLIM data base*

As described in section 1.1, the theoretical model is used to produce six preliminary data bases. Three of these runs are for sunspot minimum ($F10.7 = 70$, $Ap = 15$) during the June solstice, December solstice, and equinox seasons. The remaining three are for sunspot maximum ($F10.7 = 180$, $AP = 15$) during the same seasons. Each record of data consists of profile parameters stored for a fixed geographic (geomagnetic) point and fixed time. Each data base covers 25 latitudes (24°S–24°N, every 2°) and 48 times (0000–2330 LT, every 30 min). A subset of the SLIM data set, using a more coarse resolution for the electron density profiles ($N_e(h)$ every 4° in latitude and every hour of local time) was presented in tabular format by *Anderson et al.* [1985].

The core of the SLIM approach is to identify a relatively simple $N_e(h)$ function that will have a small number of coefficients and yet provide a good representation of the profiles calculated from the theoretical model. As guiding principles, it was decided that

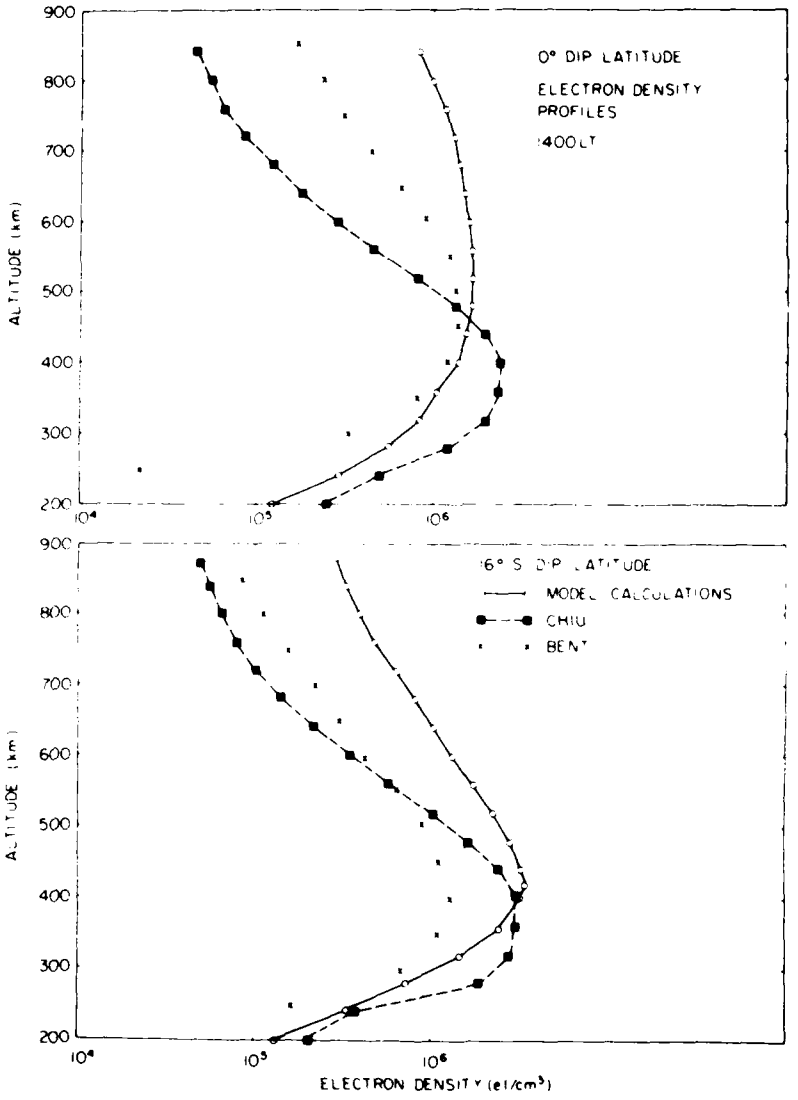

Fig. 5. A comparison between SLIM-generated electron density profiles (open circles) and the empirical models of Chiu (solid squares) and Bent (crosses) for equinox, solar cycle maximum conditions at 1400 LT. Profiles at the magnetic equator (top portion) and at 16°S dip latitude (bottom portion).

(1) maximum accuracy was required near the F region peak (in both density and height), and (2) while some errors in N_e could be accepted well below or above the peak density height (h_{max}), the overall profile (as represented by the total electron content (TEC) parameter) had to reproduce the theoretical results to within 5% or less.

The Chapman profiles developed in the earliest days of ionospheric physics offer a simple way to explain the vertical structure of plasma in the upper atmosphere. They are based on relatively simple physics and thus cannot be used to represent the entire $N_e(h)$ profiles that emerge from the more sophisticated simulation techniques in use today. As simple mathematical formulas, however, they are well suited for representing portions of the ionospheric

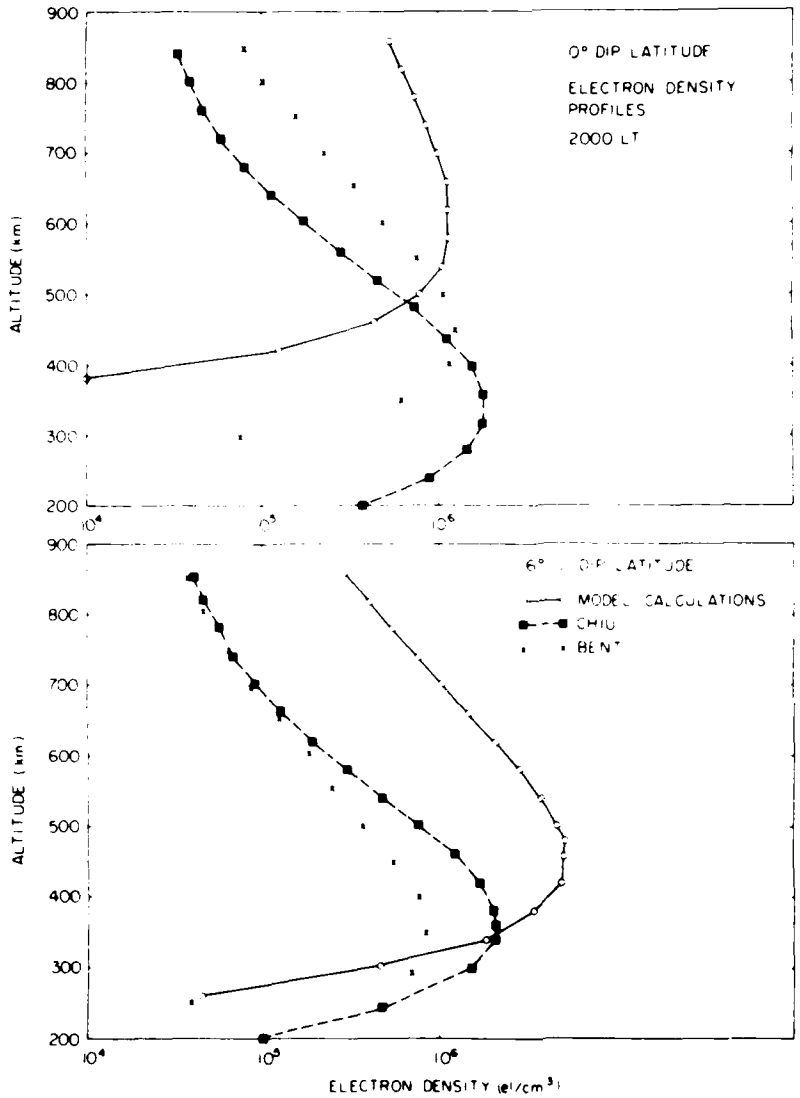

Fig. 6. A comparison between SLIM-generated electron density profiles (open circles) and the empirical models of Chiu (solid squares) and Bent (crosses) for equinox, solar cycle maximum conditions at 2000 LT. Profiles at the magnetic equator (top portion) and at 16 S dip latitude (bottom portion).

profile. Specifically, while a single Chapman profile cannot fit the entire $N_e(h)$ profile, separate Chapman formulas can be used to reproduce the topside and bottomside components of the overall profiles with good results. It was decided, therefore, to define a "generalized" or "modified" Chapman formula with coefficients that vary for each topside and bottomside component of the $N_e(h)$ profile. The function used to fit the theoretically derived profiles was thus chosen to be

$$N_e(h) = N_{max} \exp [z(1 - z - e^{-z})] \qquad (3)$$

$$z = \frac{(h - h_{max})}{A}$$

In using (3), six parameters (or coefficients) are

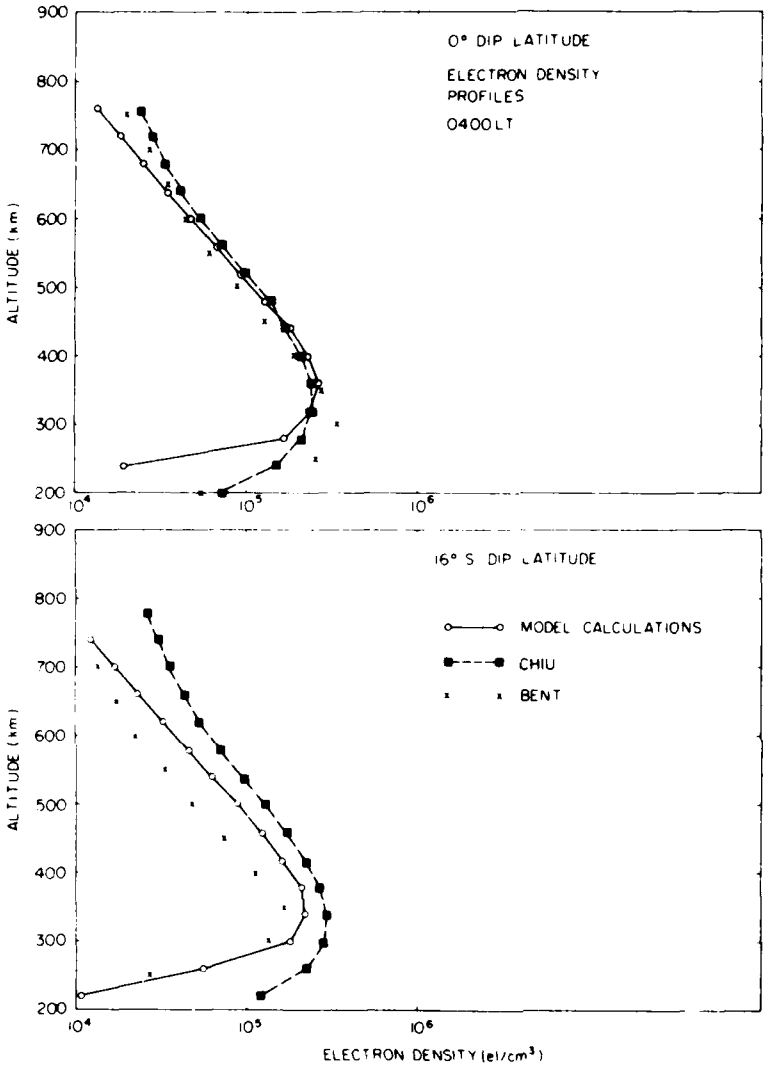

Fig. 7. A comparison between SLIM-generated electron density profiles (open circles) and the empirical models of Chiu (solid squares) and Bent (crosses) for equinox, solar cycle maximum conditions at 0500 LT. Profiles at the magnetic equator (top portion) and at 16 S dip latitude (bottom portion).

needed to reproduce the $N_e(h)$ profile: N_{max}, h_{max}, c_{up}, A_{up}, c_{lo}, A_{lo}. The advantages of this method are (1) the fit achieves 100% accuracy at N_{max} and h_{max} since they are themselves input coefficients: (2) the topside and bottomside Chapman-type functions guarantee continuity of both density and its first derivative across the fit boundary; and (3) with a fit technique weighted by density values (see below), the c and A chosen emphasize maximum accuracy in regions near the peak.

Included on each record of the database are two other numbers available for use and/or inspection. These are (1) the total electron content (TEC) obtained by integrating the SLIM profile from 180 to 1800 km; and (2) 6300-Å emission calculated from O_2^+ recombination chemistry only (and therefore, appropriate for postsunset airglow).

2.2. *Production details*

The report by *Anderson et al.* [1985] describes the numerical methods employed to obtain the parame-

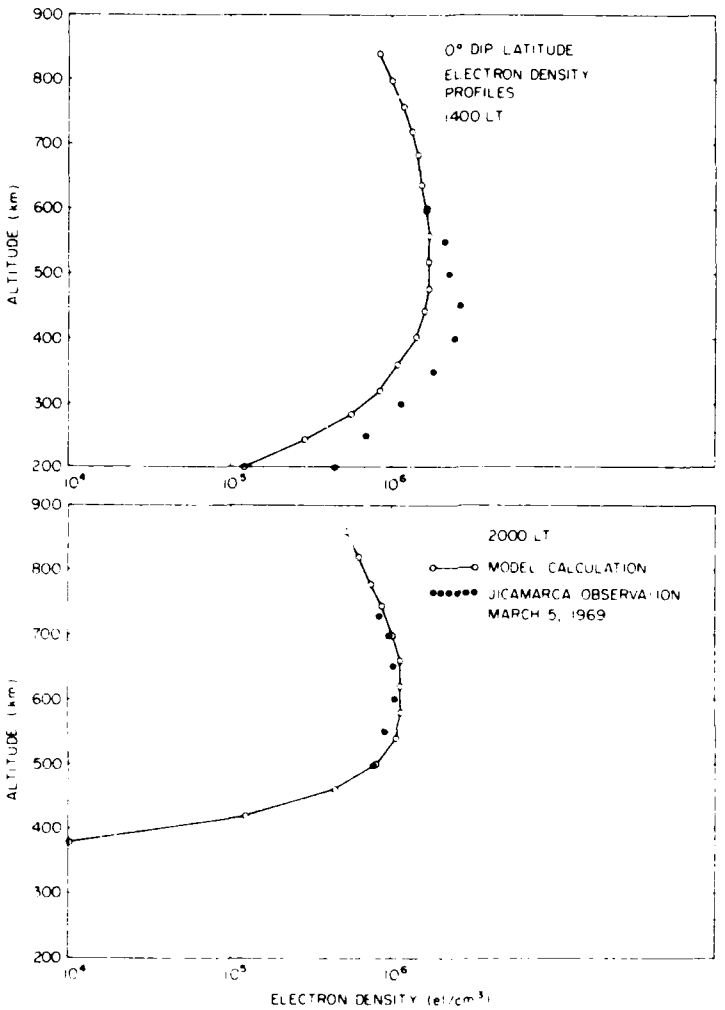

Fig. 8. A comparison between SLIM-generated electron density profiles (open circles) and profiles measured by the Jicamarca incoherent scatter radar (solid circles) on March 5, 1969, at 1400 LT (top portion) and 2000 LT (bottom portion).

ters that form the basis for SLIM. Briefly, N_{max} and h_{max} are known precisely since they are taken directly from the theoretically derived profiles; the coefficients A and c were obtained by separate least squares fits of the generalized Chapman formula to the electron densities above and below the peak.

3. COMPARISON WITH EMPIRICAL MODELS

Figure 5 compares the semi-empirical low-latitude ionospheric model (SLIM) with the Chiu and Bent models for equinox, solar maximum conditions at 1400 LT. The daytime upward **E** × **B** drift pictured in Figure 3*a* causes the broad F region profile. Respective topside scale heights at 700 km are 540 km, 150 km and 115 km. Integrations of the electron density profiles with altitude give total electron contents (TEC) of 97, 48, and 61 ($\times 10^{12}$ el/cm^2), respectively. The bottom portion of Figure 5 shows the comparison at 16 S dip latitude at the crest of the equatorial anomaly. Although the SLIM topside scale height is not as large as at the magnetic equator, it is still larger than those given by Chiu or Bent. In addition, the N_{max} value of 3.5×10^6 el/cm^3 is significantly larger than the value at the magnetic equator due to the combination of upward and poleward **E** × **B** drift

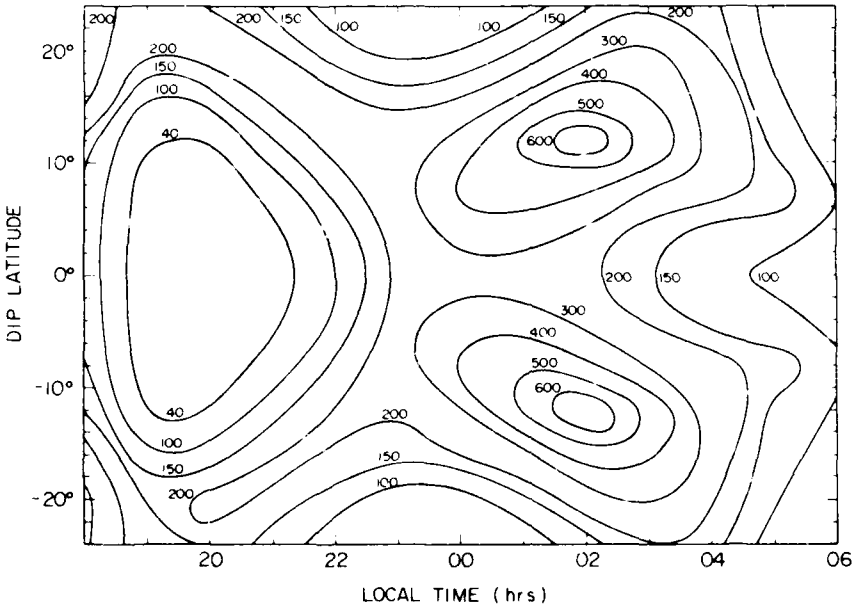

Fig. 9. Calculated 6300 Å intensity contours (Rayleighs) as a function of latitude and local time for equinox, solar cycle maximum conditions.

and downward diffusion. Note that neither the Chiu or Bent profiles shows any significant change with latitude.

The most dramatic differences between SLIM and the empirical models occur just after sunset around 2000 LT and are pictured in Figure 6. At the magnetic equator (top portion), the postsunset enhancement in upward drift lifts the F layer to 600 km compared to h_{max} values of 450 km and 350 km for the Bent and Chiu models, respectively. Such differences in h_{max} would cause significant differences in the estimated 6300-Å airglow intensity and the ion-neutral drag coefficient in the neutral momentum equation.

At 16°S dip latitude (bottom portion of Figure 6) the same upward drift causes an enhancement in N_{max}, where the calculated value is 5×10^6 el/cm^3 compared with 2×10^6 el/cm^3 for Chiu and 8×10^5 el/cm^3 for the Bent model. Respective TEC values ($\times 10^{12}$ el/cm^2) are 139, 48, and 19. Finally, Figure 7 gives a comparison between the SLIM, Chiu and Bent at 0500 LT. The calculated profiles at the magnetic equator and 16°S dip latitude are much more Chapman-like and in reasonable agreement with the empirical models in both N_{max}, h_{max} and topside scale height. The calculated value of TEC at 16°S dip latitude (bottom portion) is 5×10^{12} el/cm^3 which compares favorably with the Bent value of 3.5×10^{12} and a Chiu value of 9×10^{12} el cm^2.

Figure 8 compares electron density profiles measured on March 5, 1969, using the Jicamarca incoherent scatter radar facility with calculated density profiles at 1400 LT and 2000 LT. The comparison demonstrates that both the large daytime plasma scale height and the calculated values of h_{max} at 2000 LT are in reasonable agreement with observed values. Again, it should be emphasized that the profiles are sensitive to the vertical $\mathbf{E} \times \mathbf{B}$ drift velocity whose diurnal variation may have significant day-to-day changes.

4. COMPARISON WITH OBSERVED 6300-Å AIRGLOW INTENSITIES

Based on the SLIM density profiles and the MSIS neutral atmosphere for the equinox, solar cycle maximum case, we calculated 6300-Å airglow intensity at night using the following formula:

$$R_{(\text{rayleighs})} = \frac{A_{6300}}{10} \int_{180\text{ km}}^{1800\text{ km}} \left\{ \frac{k_1[O_2][e^-]}{A_{tot} + (k_2[N_2]) + (k_3[e^-] + (k_4[O_2])} \right\} dh \quad (4)$$

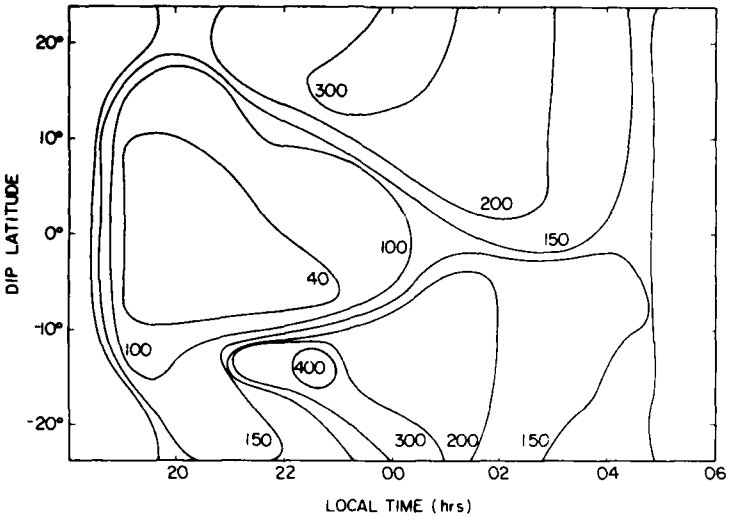

Fig. 10. Measured 6300 Å intensity contours (Rayleighs) as a function of latitude and local time under equinox, solar cycle maximum conditions [after *Abreu et al.*, 1982].

where

$k_1 = 2 \times 10^{-11} (300/T_n)^{1/2}$ cm^3 s^{-1}

[*Banks and Kockarts*, 1973];

$k_2 = 2.3 \times 10^{-11}$ cm^3 s^{-1} [*Torr and Torr*, 1982];

$k_3 = 2 \times 10^{-9}$ cm^3 s^{-1} [*Seaton*, 1955];

$k_4 = 5.3 \times 10^{-11}$ cm^3 s^{-1} [*Torr and Torr*, 1982];

$A_{tot} = 0.00681$ s^{-1} [*Torr and Torr*, 1982];

$A_{6300} = 0.00515$ s^{-1} [*Torr and Torr*, 1982];

dh = height element, km.

Figure 9 presents 6300-Å isointensity contours in Rayleighs as a function of dip latitude and local time. Near the magnetic equator, just after sunset, the intensity drops to less than 10 Rayleighs due to the high altitude (over 350 km) of the bottomside of the F layer. Peaks in airglow intensity occur at ± 16° latitude caused by the crests in ionization which occur there and the lower altitude of the F layer. As local time increases, the crests in airglow intensity move toward the magnetic equator due to downward **E** × **B** drift which lowers the F layer as it transports plasma back toward the equator. The subsequent motion of the airglow crests away from the equator after 2300 LT is due to the abatement of equatorward wind after 2200 LT which allows the F layer to move to a lower altitude thus increasing the airglow intensity.

Figure 10 presents iso-intensity contours of 6300-Å airglow based on data collected by the visible airglow experiment (VAE) on board the AE-E satellite [*Abreu et al.*, 1982]. These observations were averaged over longitude from September 1980 to November 1980 and are essentially representative of equinox, solar cycle maximum conditions. Several of the features, such as the very low airglow intensities near the magnetic equator after sunset, the crests in airglow that move toward the magnetic equator, and the subsequent motion away from the equator after 2300 LT are reproduced by the SLIM calculated airglow results. The absolute intensity levels in Rayleighs show an excellent agreement in the premidnight sector; the postmidnight enhancements are factors of the 2–3 higher in SLIM as compared to the *AE* average values (an effect due to neutral wind differences). Since 6300-Å airglow is produced near the bottomside of the F layer and is very sensitive to the height of this region, the basic agreement between calculated and observed values gives us confidence that the assumed neutral wind model and the **E** × **B** drift model are fairly realistic, at least for this season and solar cycle. A paper is in preparation which examines the separate and combined roles played by neutral wind and **E** × **B** drift in producing the ob-

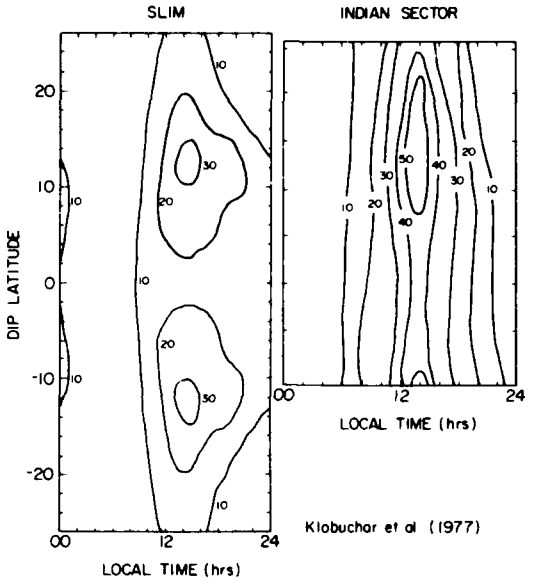

Fig. 11. Contours of calculated TEC values ($\times 10^{12}$ el.cm^2), for equinox, solar cycle minimum conditions, left; and contours of observed TEC values in the Indian sector [after *Klobuchar et al.*, 1977], right.

served latitude and local time variations in 6300-Å intensity.

5. COMPARISON BETWEEN CALCULATED AND OBSERVED TOTAL ELECTRON CONTENT VALUES

Integration of an electron density profile with altitude gives the total electron content (TEC). Figures 11 and 12 present contour plots of TEC as a function of latitude and local time calculated from the equinox, solar cycle minimum and maximum SLIM profiles (integrated over the 180–1800 km altitude range). Daytime crests in TEC values occur on either side of the equator under both minimum and maximum solar flux conditions; these correspond to crests in the peak electron density, N_{max}, having the same latitudinal distribution (the so-called equatorial anomaly). At the magnetic equator, however, there is only one daytime maximum value in TEC, in contrast to the two maxima characteristically seen in N_{max} (one in the morning and one in the afternoon). This is in agreement with observations. Using ATS-6 measurements of TEC at Ootacamund in the Indian sector, *Sethia et al.* [1978] report only one maximum in daytime TEC at the magnetic equator.

The premidnight enhancement in TEC at $\pm 10°$–$15°$ latitude results from the postsunset enhancement in upward drift and has been observed at a number of low-latitude locations, most notably at Ascension Island. Figure 13, taken from the paper by *Anderson and Klobuchar* [1983], shows the large day-to-day variation in TEC at Ascension Island for the month of September 1979. Often the premidnight maximum in TEC is greater than the daytime maximum value. Anderson and Klobuchar found that the strength of the meridional neutral wind had a strong modulating effect on the magnitude of the premidnight enhancement. A strong poleward wind in the late afternoon reduces the TEC enhancement by lowering the F layer at the crests of the anomaly.

Figures 11 and 12 also display contours of TEC for the equinoctial, solar minimum and maximum periods of 1975 and 1970 observed in the Indian subcontinent region [*Klobuchar et al.*, 1977]. The contour shapes are very similar; however, the observed magnitudes are higher during solar minimum and lower during solar maximum than the SLIM calculated TEC values. Presumably, this is because the 1970 and 1975 sunspot numbers and $F10.7$ cm flux values (and hence ionization production rates) were less extreme than the conditions assumed in the SLIM calculations.

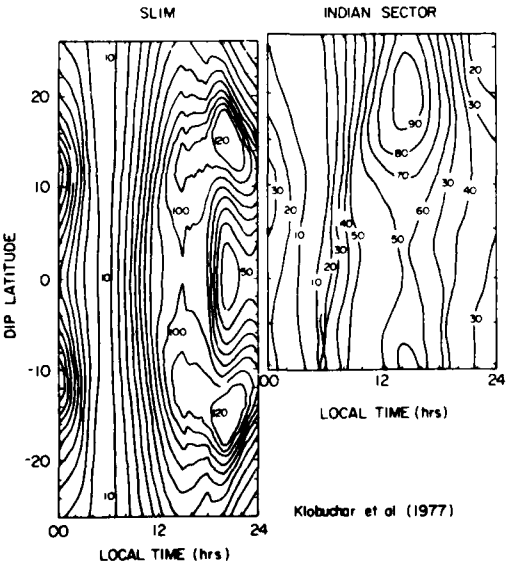

Fig. 12. Contours of calculated TEC values ($\times 10^{12}$ el/cm^2), for equinox, solar cycle maximum conditions, left; and contours of observed TEC values in the Indian sector [after *Klobuchar et al.*, 1977], right.

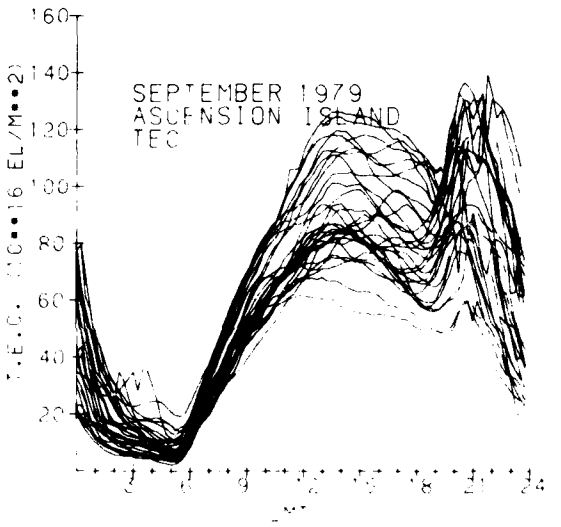

Fig. 13. Measured values of TEC versus local time at Ascension Island for several days in September 1979 [after *Anderson and Klobuchar*, 1983].

6. CONCLUSIONS

A very brief description of the generation of a semi-empirical low-latitude ionospheric model has been presented in which theoretically calculated electron density profiles are approximated by a modified Chapman function given by (3).

$$N_e(h) = N_{max} \exp [c(1 - z - e^{-z})]$$

where

$$z = \frac{h - h_{max}}{A}$$

and N_{max} and h_{max} represent the peak electron density and the altitude of the F_2 peak, respectively. Above the peak altitude, $z_{up} = (h - h_{max})/A_{up}$ and $c = c_{up}$ while below the peak, $z_{lo} = (h - h_{max})/A_{lo}$ and $c = c_{lo}$. The six coefficients which describe each profile are N_{max}, h_{max}, A_{up}, c_{up}, A_{lo} and c_{lo}. Appropriate coefficients which regenerate electron density profiles (180–1800 km), every half hour local time and every 2° dip latitude between 24°N and 24° dip latitude have been calculated. Six cases have been generated, both solstice periods and one equinox period for solar cycle minimum and solar maximum conditions. These coefficients and resultant electron density profiles are provided in *Anderson et al.* [1985] and are also available in computer readable form upon request.

A subroutine which is able to quickly generate realistic electron density profiles has a number of applications. By providing diurnal $N_e(h)$ and TEC values at any specified dip latitude or slant path, SLIM could be used to examine propagation effects determined by ionospheric structure. SLIM has several possible applications related to so-called "active experiments" where ambient ionospheric conditions need to be specified for preexperiment planning and postevent analysis. In addition, such a model would yield flux-tube integrated Pedersen conductivity and electron content values which are important in determining and predicting low-latitude instability growth rates. Finally, the program would be capable of supplying airglow intensities both in the vertical and at any slant viewing angle desired.

One final note of caution, since the theoretical calculations involve only O^+ ions, SLIM is basically an F region ionospheric model and does not give realistic electron densities below the F layer where NO^+ and O_2^+ may dominate or the topside where H^+ may be the dominant ion. Daytime and nighttime electron densities in the topside region are typically around 10^4 el/cm^3 with very large scale heights reflecting the low mass of the H^+ ion. During the day, bottomside electron and ion densities in the 110 to 180 km altitude range are 1 to 3 × 10^5 el/cm^3 and depend on solar zenith angle. At night, the low-latitude bottomside NO^+ density profiles are highly variable with F_1 region densities varying between 1 × 10^3 and 2 × 10^4 el/cm^3. It may be necessary, therefore, for the users to supply their own electron density specification in the ionospheric regions where SLIM is not valid.

APPENDIX: ANALYTIC WIND EQUATIONS

Equinox

$$V_0 = 8.61 \times 10^{-3} * \theta^2 \frac{\theta}{|\theta|}$$

$$V_{24} = 2\theta \cos \frac{2\pi}{24}\left(t - 18 - \frac{|\theta|}{7}\right)$$

$$V_{12} = 50 \sin\left(\frac{\pi}{180} * \frac{10}{3}\theta\right) \cos \frac{2\pi}{12}\left(t - 9 - \frac{|\theta|}{12}\right)$$

$$V_8 = 0.38\theta \cos \frac{2\pi}{8}(t - 8.2 + 0.079|\theta|)$$

$$V_{TOT} = V_0 + V_{24} + V_{12} + V_8$$

The θ is latitude in degrees.

December solstice

$$V_0 = 3.116 \times 10^{-4} * \theta^2(\theta + 45) - 49$$

$$V_{24} = 2\theta_{24} \cos \frac{2\pi}{24}\left(t - 18 - \frac{|\theta_{24}|}{7}\right) \qquad \theta_{24} = \theta + 10$$

$$V_{12} = 50 \sin\left(\frac{\pi}{180} * \frac{10}{3}\theta\right) \cos \frac{2\pi}{12}\left(t - 9 - \frac{|\theta|}{12}\right)$$

$$V_8 = 0.38\theta \cos \frac{2\pi}{8}(t - 8.2 + 0.079|\theta|)$$

$$V_{TOT} = V_0 + V_{24} + V_{12} + V_8$$

June solstice

$$V_0 = -3.116 \times 10^{-4} * \theta^2(45 - \theta) + 49$$

$$V_{24} = 2\theta_{24} \cos \frac{2\pi}{24}\left(t - 18 - \frac{|\theta_{24}|}{7}\right) \qquad \theta_{24} = \theta - 10$$

$$V_{12} = 50 \sin\left(\frac{\pi}{180} * \frac{10}{3}\theta\right) \cos \frac{2\pi}{12}\left(t - 9 - \frac{|\theta|}{12}\right)$$

$$V_8 = 0.38\theta \cos \frac{2\pi}{8}(t - 8.2 + 0.079|\theta|)$$

where

$$V_{TOT} = V_0 + V_{24} + V_{12} + V_8 \qquad \text{(m/s)}$$

and t is hours, local time; θ is geographic latitude, positive northern hemisphere.

Acknowledgments. We would like to thank Jeffrey Forbes, Bela Fejer, Leo McNamara, John Klobuchar and Jeffrey Baumgardner for numerous discussions and their helpful suggestions. We also wish to thank Betsy Hodges for her help in manuscript typing and preparation. This research was supported in part by AFGL contact F19628-81-K-0051 with Boston University. Michael Hicks produced the graphs using the RS/1 package on the Boston University Department of Astronomy VAX-11/750. Thanks also to the staff of the AFGL Computer Center for their help.

REFERENCES

Abreu, V. J., G. A. Schmitt, P. B. Hays, and T. P. Dachev, Volume emission rate profiles of the 6300-A tropical nightglow obtained from the AE-E satellite: Latitudinal and seasonal variations, *J. Geophys. Res.*, *87*, 6346–6352, 1982.

Anderson, D. N., A theoretical study of the ionospheric *F*-region equatorial anomaly, II, Results in the American and Asian sectors, *Planet. Space Sci.*, *21*, 421–442, 1973.

Anderson, D. N., Modeling ambient low-latitude *F*-region ionosphere—A review, *J. Atmos. Terr. Phys.*, *43*, 753–762, 1981.

Anderson, D. N., and J. A. Klobuchar, Modeling the total electron content observations above Ascension Island, *J. Geophys. Res.*, *88*, 8020–8024, 1983.

Anderson, D. N., M. Mendillo, and B. Herniter, A semi-empirical low-latitude ionospheric model, *AFGL Tech. Rep. RT-85-0254*, Air Force Geophys. Lab., Hanscom Air Force Base, Mass., 1985.

Banks, P. M., and G. Kockarts, *Aeronomy*, part A, p. 260, Academic, Orlando, Fla., 1973.

CCIR, International Radio Consultative Committee atlas of ionospheric characteristics, Rep. 340-3, in *Recommendations and Reports of the CCIR*, vol. 6, International Telecommunications Union, Geneva, 1978.

Chiu, Y. T., An improved phenomenological model of ionospheric density, *J. Atmos. Terr. Phys.*, *37*, 1563–1570, 1975.

Fejer, B. G., D. T. Farley, R. F. Woodman, and C. Calderon, Dependence of equatorial *F* region vertical drifts on season and solar cycle, *J. Geophys. Res.*, *84*, 5792–5796, 1979.

Fejer, B. G., D. T. Farley, C. A. Gonzales, R. F. Woodman, and C. Calderon, *F* region east-west drifts at Jicamarca, *J. Geophys. Res.*, *86*, 215–218, 1981.

Forbes, J. R., Atmospheric tides, 1, Model description and results for the solar diurnal component, *J. Geophys. Res.*, *87*, 5222–5240, 1982*a*.

Forbes, J. R., Atmospheric tides, 2, The solar and lunar semidiurnal components, *J. Geophys. Res.*, *87*, 5241–5252, 1982*b*.

Hanson, W. B., and R. J. Moffet, Ionization transport effects in the equatorial *F* region, *J. Geophys. Res.*, *71*, 5559–5572, 1966.

Hedin, A. E., A revised thermospheric model based on mass spectrometer and incoherent scatter data: MSIS-83, *J. Geophys. Res.*, *88*, 10,170–10,188, 1983.

Kendall, P. C., and W. M. Pickering, Magnetoplasma diffusion at *F*2-region altitudes, *Planet. Space Sci.*, *15*, 825–833, 1967.

Klobuchar, J. A., K. N. Iyer, H. O. Vats, and R. G. Rastogi, A numerical model of equatorial and low latitude total electron content for use by tracking systems for ionospheric corrections, *Indian J. Radio Space Phys.*, *6*, 159–164, 1977.

Llewellyn, S. K., and R. B. Bent, Documentation and description of the Bent ionospheric model, *Rep. AFCRL-TR-73-0657, AD 772733*, Air Force Cambridge Res. Lab., Bedford, Mass., 1973.

McNamara, L. F., Prediction of total electron content using the International Reference Ionosphere, *Adv. Space Res.*, *4*, 25–50, 1984.

Moffett, R. J., The equatorial anomaly in the electron distribution of the terrestrial *F*-region, *Fundam. Cosmic Phys.*, *4*, 313–391, 1979.

Rawer, K., *International Reference Ionosphere—IRI79*, edited by J. V. Lincoln and R. O. Conkright, World Data Center A, NOAA, Boulder, Colo., 1981.

Roble, R. G., R. E. Dickinson, and E. C. Ridley, Seasonal and solar cycle variations of the zonal mean circulation in the thermosphere, *J. Geophys. Res.*, *82*, 5493–5504, 1977.

Seaton, M. S., The calculation of cross-sections for excitation of forbidden transition lines by electron impact, *J. Atmos. Terr. Phys., Spec. Suppl.*, *5*, 289–301, 1955.

Sethia, G., H. Chandra, M. R. Deshpande, R. G. Rastogi, B. S. Murthy, and K. Davies, Total electron content from ATS-6 group delay measurements at Ootacamund, India, 14-1, 14-7, paper presented at Symposium of the COSPAR Satellite

Beacon Group, Comm. on Space Res., Firenze, Italy, May 22–25, 1978.

Torr, M. R., and D. G. Torr, Chemistry of the thermosphere and ionosphere, *J. Atmos. Terr. Phys.*, *41*, 797 839, 1979.

Torr, M. R., and D. G. Torr, The role of metastable species in the thermosphere, *Rev. Geophys.*, *20*(1), 91–144, 1982.

Woodman, R. F., Vertical drift velocities and east-west electric fields at the magnetic equator, *J. Geophys. Res.*, *75*, 6249 6259, 1970.

D. N. Anderson, Air Force Geophysics Laboratory, Hanscom Air Force Base, MA 01731.

B. Herniter and M. Mendillo, Astronomy Department, Boston University, 725 Commonwealth Avenue, Boston, MA 02215.